Local Structure and Photochromic Response in Ormosils Containing Dodecatungstophosphoric Acid

M. de Oliveira Jr.,[†] A. Lopes de Souza,[†] J. Schneider,*,[†] and U. Pereira Rodrigues-Filho[‡]

[†]*Instituto de Física de São Carlos and* [‡]*Instituto de Química de São Carlos, Universidade de São Paulo, Av. Trabalhador São-carlense 400, CEP 13566-590, São Carlos, SP, Brazil*

Received August 5, 2010. Revised Manuscript Received November 20, 2010

Two hybrid materials based on dodecatungstophosphoric acid (HPW) dispersed in ormosils modified with 3-aminopropiltrietoxysilane (APTS) or with *N*-(3-(trimethoxysilyl)-propyl)-ethylene-diamine (TSPEN) show reversible photochromic response induced by irradiation in the $200-390$ nm UV range. A set of solid-state nuclear magnetic resonance (NMR) techniques was used to analyze the structural properties of the main components of these hybrids (the HPW polyanion, the inorganic matrix, and the organic functionalities). For the ormosils, the use of ^{29}Si NMR, $\{^1H\}$-^{29}Si cross-polarization, and $\{^1H\}$-^{29}Si HETCOR revealed a homogeneous distribution of silicon species Q^n, T^2, and T^3 for the APTS hybrid, contrasting with the separation of T^3 species in the TSPEN hybrid. The combination of ^{31}P NMR, $\{^1H\}$-^{31}P cross-polarization and ^{31}P-$\{^1H\}$ spin—echo double resonance (SEDOR) revealed the dispersion of the HPW ions in the ormosil, occupying sites with a high number of close protons (>50). Differences in the molecular dynamics at room temperature, inferred from SEDOR experiments, indicate a state of restricted mobility of the HPW ion and the surrounding molecular groups in the TSPEN hybrid. This behavior is consistent with the presence of more amino groups in the TSPEN, acting as chelating groups to the HPW ion. This hybrid, with the strong chelate interaction of the diamine group, shows the most intense photochromic response, in agreement with the charge transfer models proposed to explain the photochromic effect. Electronic reflectance spectroscopy in irradiated samples revealed the presence of one-electron and two-electron reduced polyanions. The one-electron reduced species could be detected also by ^{31}P NMR spectroscopy immediately after UV irradiation.

1. Introduction

Photochromic materials have potential technological applications in optical lenses and smart windows,[1,2] information displays, high-density memory devices,[3] and UV dosimetry.[4] Polyoxometalates (POM) are good candidates for the preparation of such materials because once irradiated with ultraviolet light they form colored species, known as heteropolyblues or heteropolybrowns.[5–7] Among the polyoxometalates are the Keggin heteropolymetalates with formula $[XM_{12}O_{40}]^{n-}$, where X are called heteroatoms in the center of the structure and M are addenda atoms arranged in MO_6 in C_{4v} microsymmetry. The most common addenda atoms are W, Mo, and V in high oxidation states. These Keggin heteropolymetalates are the most prominent POM photochromic dyes. Keggin heteropolyblues and heteropolybrowns are reduced POMs belonging to class II mixed valence compounds, according to the classification of Robinson and Davy.[8] Heteropolyblues can be reoxidized since the injected electrons go to nonbonding orbitals, formed by the nd of the W or Mo orbitals, delocalized in the addenda atoms. However, the heteropolybrowns are irreversibly reduced heteropolymetalates by accepting six electrons and creating three W^{4+}, forming in this way a metal—metal bond triad.[9] However, to be able to use these photochromic dyes in useful devices, matrix materials with adequate optical, mechanical, and chemical properties should be developed. Hybrid materials are a promising option, combining the advantages of organic and ceramic materials.[10,11]

*Corresponding author. Phone: 55-16-3373-9600. Fax: 55-16-3373-9876. E-mail: schnei@ifsc.usp.br.

(1) Ford, C.; Mc Climans, P. Curable coating composition for forming impact resistant, abrasion and/or scratch resistant photochromic article, comprises unblocked polyisocyanate terminated polyurethane pre-polymer, polyol, and photochromic agent. Patent numbers US2008067701-A1, WO2008031879-A1, EP2066714-A1, US7662433-B2, Mar. 20, 2008.
(2) Wiand, R. C. Glass laminate for use in e.g. automotive vehicle, has glass sheet with surface having optically clean resin layer bonded with adhesive layer, where clean resin or pressure sensitive adhesive has photochromic moiety. Patent numbers WO2008020829-A2, WO2008020829-A3, Feb. 21, 2008.
(3) Zhao, L.; Sui, D.; Chai, J.; Wang, Y.; Jiang, S. *J. Phys. Chem. B* **2006**, *110*, 242990.
(4) Parisi, A. V.; Kimlin, M. G.; Turnbull, D. J.; Macaranas, J. *Photochem. Photobiol. Sci.* **2005**, *4*, 907.
(5) Pope, M. T. *Heteropoly and Isopoly Oxometalates*; Springer-Verlag: Berlin, 1983.
(6) Papacontantinou, E. *Chem. Soc. Rev.* **1989**, *18*, 1.
(7) Yamase, T. *Chem. Rev.* **1998**, *98*, 307.

(8) Borrfis-Almenar, J. J.; Clemente, J. M.; Coronado, E.; Tsukerblat, B. S. *Chem. Phys.* **1995**, *195*, 1.
(9) Dickman, M. H.; Ozeki, T.; Evans, H. T.; Rong, C. Y.; Jameson, G. B.; Pope, M. T. *J. Chem. Soc., Dalton Trans.* **2000**, *2*, 149.
(10) Sanchez, C.; Lebeau, B.; Chaputt, F.; Boilot, J. P. *Adv. Mater.* **2003**, *15*, 1969.

Among the hybrid materials, organically modified silicas (ormosils) prepared by the sol−gel process are the natural choice to develop devices based on POM due to the possibility to easily incorporate these ions in the hybrid by a bottom-up procedure. Also, the intermolecular interactions of POM ions with different organic functionalities may be used to tune the ormosil properties.[12,13]

The photochromic response of the POM ions is based on their photoreduction, which depends on their redox potential, the pH of the medium, and the type of organic electron donor.[6] Yamase[7] has advanced an explanation for the photochromic behavior of alkylammonium POM proposing a charge transfer state formed by the photo-excited POM and the alkylammonium groups. Lu et al.,[14] using atomic force microscopy and transmission electron microscopy, demonstrated that a reversible photochromic film based on phosphotungstic acid (HPW) in polyacrylamide host undergoes morphological changes as the irradiation time increases. This morphological change was ascribed to the agglomeration of HPW nanometric particles and concomitant polymer cross-linking. The cross-linking of the polymeric structure occurs after the transference of a proton from the polyacrylamide to a bridging oxygen in the excited HPW anion (W−O−W) resulting in a radical formation, thus starting the chain propagation of the cross-linking reaction.[15] Carls et al.[16] observed similar photoinduced electrons and proton transfer in a spun-cast low molecular weight, $M_w = 14\,000$, poly(vinyl alcohol) (PVA)−HPW hybrid material used as photoresist. The photochemical oxidation of the PVA was observed in several polyoxometalate−PVA solutions[17] displaying interesting oscillatory kinetics. Another method to develop a suitable matrix environment for POM based photoactive devices is the electrostatic layer-by-layer technique, producing multilayer films with reversible photochromic behavior.[18]

Considering hybrid ormosil matrices, instead of polymeric, there are few reports of nanocomposite films with reversible photochromism based on POM such as phosphomolybdate,[19] phosphotungstate,[19−21] or silicotungstate[19,22] used in ormosils bearing 3-aminopropyltriethoxysilane (APTS) and tetraethylorthosilicate (TEOS).

Hybrid materials are usually classified as type I or II, depending on whether there is no chemical bonding among the organic and inorganic parts or if they are chemically connected. Ormosils are likely to belong to the class II since the organic functionalities are introduced through organosilanes that react with the tetraalkylorthosilicate, used to generate the inorganic silica network. HPW has been incorporated in ormosils prepared from TEOS and tetraethyleneglycol.[23] Huang et al.[24] reported a thermally initiated class II hybrid material bearing sorbed silicotungstate with metracylamide and vinyl functionalities, resulting in a reversible photochromic nanocomposite. The organic groups inside the ormosil materials seem to play an important role in coloration and discoloration mechanism; however, this effect was exploited more systematically with organic photochromic dyes.[25]

In the present work we have studied some class II hybrid materials based on HPW−amino modified silica ormosils, where the amino groups were added using APTS or *N*-(3-(trimethoxysilyl)-propyl)-ethylenediamine (TSPEN). These two hybrids show photochromic response to UV in the region 200 nm to 390 nm, turning blue after irradiation. The structure of these ormosils is constituted of three main parts: the inorganic silica matrix, responsible for mechanical properties; the HPW polyanion, responsible for the photochromic response; and the organic functionalities providing absorption sites, protons, and electrons to HPW during the reduction process induced by irradiation. The aim of this study is to obtain a structural description of the different parts of a photochromic ormosil and their mutual interaction, using a set of multinuclear high-resolution solid-state nuclear magnetic resonance (NMR) techniques. The structural picture determined from this procedure is relevant to understanding the influence of the organic functionalities on the photochromic effect. ^{29}Si and ^{13}C NMR were applied to analyze the extent of sol−gel reactions, determining the presence of organic molecular groups attached to Si. ^{29}Si NMR is especially suitable to describe the state of condensation of the ormosil silicate network, determining the type and fraction of silicon species. Double resonance techniques based on the heteronuclear magnetic dipolar coupling, such as {^{1}H}-^{29}Si cross-polarization (CP) and {^{1}H}-^{29}Si heteronuclear correlation (HETCOR) may provide information on the relative spatial distribution of silicon species and to detect possible heterogeneities in the ormosil network. ^{31}P NMR techniques are well established as sensitive to the structural changes of the POM polyanion or its coordination environment in solution[26] and in the solid state.[27−31]

(11) Babonneau, F.; Thorne, K.; Mackenzie, J. D. *Chem. Mater.* **1989**, *1*, 554.
(12) Zhang, X.; Wu, W.; Wang, J.; Liu, C.; Qian, S. *J. Mater. Res.* **2008**, *23*, 18.
(13) Huang, Y.; Pan, Q. Y.; Dong, X. W.; Cheng, Z. X. *Mater. Chem. Phys.* **2006**, *97*, 431.
(14) Feng, W.; Zhang, T. R.; Liu, Y.; Lu, R.; Zhao, Y. Y.; Yao., J. N. *J. Mater. Sci.* **2003**, *38*, 1045.
(15) He, T.; Yao, J. *Prog. Mater. Sci.* **2006**, *51*, 810.
(16) Carls, J. C.; Argitis, P.; Helle, A. *J. Electrochem. Soc.* **1992**, *139*, 786.
(17) Ostroushko, A. A.; Sennikov, M. Y. *Russ. J. Phys. Chem. A* **2009**, *83*, 111.
(18) Xu, B.; Xu, L.; Gao, G.; Guo, W.; Liu, S. *J. Colloid Interface Sci.* **2009**, *330*, 408.
(19) Rui, Z. T.; Feng, W.; Bao, C. Y.; Lu, R.; Zhang, X. T.; Li, T. J.; Zhao, Y. Y.; Yao, J. N. *J. Mater. Res.* **2001**, *16*, 2256.
(20) Zhang, T. R.; Feng, W.; Lu, R.; Zhang, X. T.; Jin, M.; Li, T. J.; Zhao, Y. Y.; Yao, J. N. *Thin Solid Films* **2002**, *402*, 237.
(21) Zhang, T. R.; Feng, W.; Lu, R.; Bao, C. Y.; Li, T. J.; Zhao, Y. Y.; Yao, J. N. *Mater. Chem. Phys.* **2002**, *78*, 380.
(22) Zhang, T. R.; Jin, M.; Feng, W.; Lu, R.; Bao, C. Y.; Zhao, Y. Y.; Li, T. J.; Yao, J. N. *Chem. J. Chin. Univ.* **2002**, *23*, 1979.
(23) Judeinstein, P.; Oliveira, P. W.; Krug, H.; Schmidt, H. *Chem. Phys. Lett.* **1994**, *220*, 35.
(24) Huang, Y.; Pan, Q. Y.; Dong, X. W.; Cheng, Z. X. *Mater. Chem. Phys.* **2006**, *97*, 431.
(25) Pardo, R.; Zayat, M.; Levy, D. *J. Photochem. Photobiol. A* **2008**, *198*, 232.
(26) Thouvenot, R.; Tézé, A.; Contant, R.; Hervé, G. *Inorg. Chem.* **1988**, *27*, 524.
(27) Jorris, T.; Kozik, M.; Casán-Pastor, N.; Domaille, P.; Finke, R.; Miller, W.; Baker, L. *J. Am. Chem. Soc.* **1987**, *109*, 7402.

The techniques of $\{^1H\}$-^{31}P CP and $\{^1H\}$-^{31}P spin—echo double resonance (SEDOR), based on the magnetic coupling of ^{31}P with ^1H, may provide useful insights on the proton environments around the HPW polyanions. The analysis of these chemical environments is potentially important, because the photochromic response depends critically on the strong interaction between the HPW polyanion and the neighboring proton donor groups. Moreover, one interesting possibility is the application of ^{31}P NMR in irradiated samples to identify differences in the electronic environment around the central phosphorus, related to the photochromic effect. The photochromic response of these materials was characterized by electronic reflectance spectroscopy, as a function of the UVB dose.

2. Experimental Section

2.1. Chemical. Hydrated dodecatungstophosphoric acid (HPW), 3-aminopropyltriethoxysilane (APTS), and tetraethylorthosilicate (TEOS) were purchased from Sigma-Aldrich. *N*-(3-(trimethoxysilyl)-propyl)-ethylenediamine (TSPEN) was purchased from Acros, and acetone (99.5%) was purchased from Synth. All reagents were used as received without further purification. Glass slides of 4 cm^2 were cleaned by the RCA procedure.[32] The slides were immersed in a solution 1:1:5 (v:v:v) of $NH_4OH/H_2O_2/H_2O$ for 30 min at 80 °C. After that, they were rinsed with deionized water and dried with a stream of nitrogen gas.

2.2. Ormosils Preparation. A quantity of 0.25 mmol of one of the aminoalkoxysilanes (58 μL of APTS or 54 μL of TSPEN), 0.26 mmol (59 μL) of TEOS, 0.038 mmol (0.11 g) of HPW, and 1 mL of hydrochloric acid (concentration 36−38 wt %) were added to 50 mL of acetone, under vigorous stirring. Xerogel films of each ormosil were prepared spreading the mixture on glass substrates and waiting until complete drying at room temperature. This process was repeated five times for each type of ormosil. The typical thicknesses of the films analyzed in this work were 2.2 ± 0.4 μm. Thicker films display higher sensibility to UV dose, but they are mechanically less stable and have much longer decoloration times. For NMR studies, samples in powder form were obtained after drying up each mixture at room temperature.

2.3. Experimental Techniques. The ex situ measurements of the photochromic effect of the samples were carried out using a 16S-150W solar light simulator (Solar Light Co., USA) with maximum power of 150 W equipped with an automatic shutter, controlled by a radiometer PMA2100 equipped with PMA 2110 UVA and PMA 2106 UVB detectors. The solar light simulator delivers a 5 cm UV spot to a sample positioned 7.3 cm away from the UV source. The thermal and visible radiation below 430 nm is removed by a set of internal filters. This experimental setup allows precise dose control during irradiation cycles. The UVB dose is reported on Minimal Erythema Dose (MED), that is, 21 mJ·cm^{-2}, as set by the Solar Light Company. Electronic

reflectance spectroscopy of the ormosils, deposited as films on glass, was carried out using a portable USB 4000 spectrometer (Ocean Optics, FL, U.S.A.) equipped with a fiber optic reflectance probe (R400-7-Vis-NIR) and a LS1 tungsten halogen lamp. These experiments were conducted after the UV irradiation of the samples. The fiber probe is assembled in such way that one central fiber delivers light and six surrounding fibers collect the reflected light. The samples were fixed with screws on a universal sample stage RTL-T. The optical fiber was positioned 3 mm above the surface at normal incidence, under a black metallic cover to isolate it from room light. From the reflectance spectra, integrated intensities of bands were obtained by multiple Gaussian fitting to the experimental spectra. Samples of irradiated ormosils were also prepared for ^{31}P NMR spectroscopy. In this case, the powders were dispersed on a glass plate and irradiated using a 80 W mercury vapor lamp, delivering a UVB dose of 32 MED.

High-resolution NMR experiments were performed on a magnetic field of 9.4 T with a Varian Unity INOVA spectrometer, using magic angle spinning (MAS) up to 7 kHz. The MAS experiments were carried out in a 7 mm double-resonance Varian-Jakobsen probe with silicon nitride and zircon rotors. The ^{31}P and ^{29}Si spectra were obtained from single pulse experiments (SPE), with $\pi/2$ duration of 4.0 μs, MAS at 2 kHz and 5 kHz, and recycle delays of 100 s and 300 s, respectively. Typical numbers of scans were 256 for ^{29}Si and 96 for ^{31}P. Cross-polarization MAS (CP MAS) experiments from ^1H to ^{29}Si, ^{31}P, and ^{13}C were carried out using typical $\pi/2$ pulse durations for ^1H between 3.0 to 4.5 μs, contact times between 1.0 and 25 ms, and number of scans between 1024 to 4000.

Spin—echo double resonance (SEDOR)[33] $\{^1H\}$-^{31}P NMR experiments were carried out at room (21 °C) and low (−80 °C) temperatures in a 7 mm static probe from Doty Scientific Inc. The SEDOR sequence with fixed time to the echo was used,[34,35] as shown in Figure 4. Instead of the initial $\pi/2$ pulse, a $^1H{\rightarrow}^{31}P$ CP block was used in these experiments to optimize measurement time and signal-to-noise ratio. The recycle delay (5 s) was determined by the spin—lattice relaxation of ^1H magnetization, which is faster than the ^{31}P relaxation. A contact time of 2 ms was used in all experiments, corresponding to the maximum in the CP signal. The Hahn echo for ^{31}P was created by applying the π-pulse at a fixed time $t_E = 200\ \mu$s after the CP cycle. A dephasing π-pulse is applied on ^1H at a time τ during the initial evolution period t_E, and the intensity $S(\tau)$ of the echo is recorded for values of $\tau < t_E$. The advantage of this fixed t_E sequence with respect to the conventional one is that the measured $S(\tau)$ response is governed solely by the heteronuclear coupling and it is independent of the spin—echo decay associated with homonuclear coupling. The amount of the echo intensity decrease, due to dephasing by heteronuclear coupling, is expressed in relative terms as $S(\tau)/S_0$, with S_0 the echo intensity measured in the absence of defocusing pulse on ^1H. The π-pulse durations for ^{31}P and ^1H were 8.4 and 9.5 μs respectively, and a number of scans between 256 and 320 was used.

Heteronuclear correlation (HETCOR) experiments between the pairs $\{^1H\}$-^{29}Si were performed using the solid-state sequence reported by Fyfe et al.[36] The 2D experiments were carried out

(28) Petterson, L.; Andersson, I.; Selling, A.; Grate, J. *Inorg. Chem.* **1994**, *33*, 982.
(29) Ganapathy, S.; Fournier, M.; Paul, J. F.; Delevoye, L.; Guelton, M.; Amoureux, J. P. *J. Am. Chem. Soc.* **2002**, *124*, 7821.
(30) Kazansky, L. P.; McGarvey, B. R. *Coord. Chem. Rev.* **1999**, *188*, 157.
(31) Contant, R.; Abbessi, M.; Thouvenot, R.; Hervé, G. *Inorg. Chem.* **2004**, *43*, 3597.
(32) Donley, C.; Dunphy, D.; Paine, D.; Carter, C.; Nebesny, K.; Lee, P.; Alloway, D.; Armstrong, N. R. *Langmuir* **2002**, *18*, 450.

(33) Po-Kang, W.; Slichter, C. P.; Sinfelt, J. H. *Phys. Rev. Lett.* **1984**, *53*, 82.
(34) Brunner, E.; Stemberg, U. *Prog. Nucl. Magn. Reson. Spectrosc.* **1998**, *32*, 21.
(35) Ueda, T.; Tatsumi, T.; Eguchi, T.; Nakamura, N. *J. Phys. Chem. B* **2001**, *105*, 5391.
(36) Fyfe, C. A.; Zhang, Y.; Aroca, P. *J. Am. Chem. Soc.* **1992**, *114*, 3252.
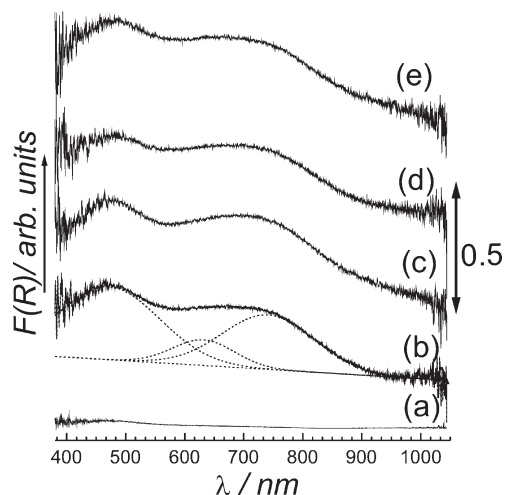
Figure 1. Reflectance electronic spectra of the HCl/HPW/APTS ormosils as a function of the UVB dose, (a) 4.90 MED, (b) 9.70 MED, (c) 19.4MED, (d) 48.6 MED, (e) 97.2 MED. Dot lines in (b): representative least-squares Gaussian fitting.

using dwell times for ^{1}H evolution between 5 and 11 μs with up to 128 increments, 1200 scans, 3 s recycle delay, $\pi/2$ ^{1}H pulse of 4.2 μs and MAS of 5 kHz. A phosphoric acid solution (H$_3$PO$_4$ 85%) was used as standard for ^{31}P chemical shift. Solid samples of kaolinite (−91.5 ppm) and adamantane (CH at 38.6 ppm) were used, respectively, for referencing ^{29}Si and ^{13}C relative to tetramethylsilane (TMS).

3. Results

3.1. Electronic Spectroscopy. The APTS/HPW and the TSPEN/HPW ormosils displayed a bluish color after UV irradiation, ranging from light blue to dark blue according to the increase in UV dose. In order to quantify the UV photochromic response, reflectance electronic (UV−Vis) spectra were taken after each UV dose essayed. Figures 1 and 2 show the spectra for each ormosil film as a function of the UV dose. Both set of spectra were fitted with three Gaussian functions, with quite similar peak positions in both ormosils and a straight baseline. This choice for the numerical analysis is based on the assignments proposed in the literature.[9,37,38] According to these studies, the wavelengths and relative intensities for bands from [PW$_{12}$O$_{40}$]$^{4-}$ are 1250 nm (1600), 752 nm (2000), and 487 nm (2000), while [PW$_{12}$O$_{40}$]$^{5-}$ has bands at 1111 nm (3000), 653 nm (4400), and 487 nm (3300). All these data were collected in 1.0 M sulfuric acid solutions.

APTS samples displayed three dose-independent Gaussian components at 631 nm, 740 nm, and 471 nm, listed in order of increasing intensity. In contrast, the TSPEN based ormosil showed three dose-dependent bands. The spectrum collected after irradiation with 4.9 MED showed the most intense peak at 480 nm, a less intense one at 745 nm, and the smallest one at 635 nm, similar to irradiated APTS ormosil. As the dose increases, the peak at 745 nm shows an increase in intensity and a small red shift, while the other two peaks shift to lower wavelengths.
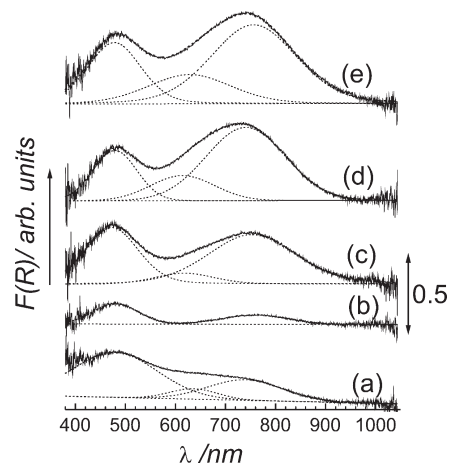
(37) Varga, G. M., Jr.; Papaconstainnou, E.; Pope, T. *Inorg. Chem.* **1970**, *9*, 662.
(38) He, T.; Yao, J. *Prog. Mater. Sci.* **2006**, *51*, 810.

Figure 2. Reflectance electronic spectra of the HCl/HPW/TSPEN ormosils as a function of the UVB dose, (a) 4.90 MED, (b) 9.70 MED, (c) 19.4MED, (d) 48.6 MED, (e) 97.2 MED. Dot lines: least-squares Gaussian fittings.
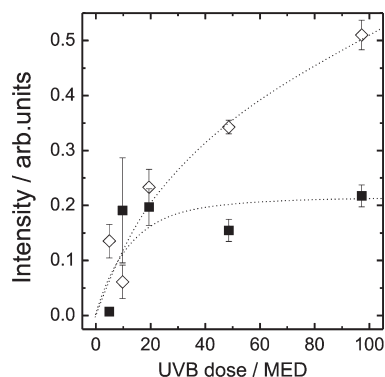

Figure 3. Intensity of the fitted band with the longest wavelength in the reflectance electronic spectra for the APTS (■) and TSPEN (◇) ormosils as a function of the UVB dose. Dashed lines: guides to the eye.

These three peaks observed in the electronic spectra of both ormosils are quite close to the peaks observed for the mono- and bireduced heteropolyblue species.[37,38] The 480 nm peak has the contribution of both heteropolyblues, [PW$_{12}$O$_{40}$]$^{4-}$ and [PW$_{12}$O$_{40}$]$^{5-}$. The 631 nm peak is assigned to the [PW$_{12}$O$_{40}$]$^{5-}$ while the 710 nm and 740 nm peaks were assigned to the [PW$_{12}$O$_{40}$]$^{4-}$. All bands are mixed-valence charge transfer bands from d orbitals in the W^V center toward the d orbitals of the W^{VI} center.

To quantify the response of the electronic spectrum to the irradiation, the intensity of the peak at the longest wavelength was plotted as a function of the UVB dose in Figure 3, for each ormosil. This peak was chosen because it has the lowest uncertainty during the fitting procedure: it is well-defined within the acquisition window of the spectrophotometer and has less overlap than the other two peaks. The error bars in Figure 3 correspond to the average deviation from a set of five independent sample preparations, measurements, and fittings. For the APTS ormosil, the data in Figure 3 show an initial increment of the band intensity and a nearly constant response above 20 MED. In contrast, a progressive increment of the intensity is observed for the TSPEN ormosil, which may be a more suitable response for applications in UV
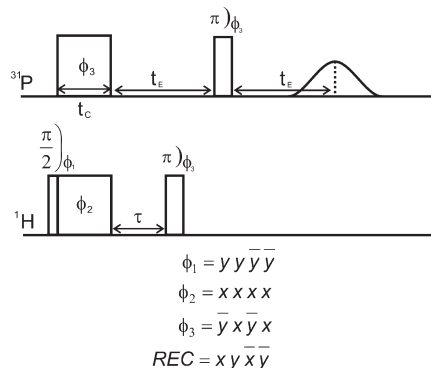
Figure 4. ^{1}H→^{31}P CP ^{31}P{^{1}H}SEDOR pulse sequence and minimum phase cycling table. Phase ϕ_3 for pulses in the observe channel can be fully cycled. REC: phase of the receiver.
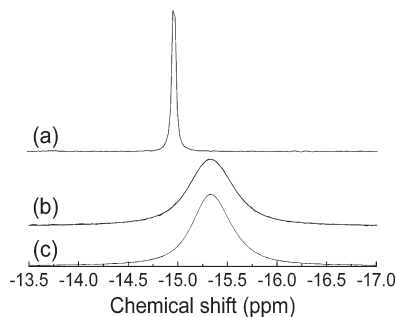

Figure 5. ^{31}P NMR spectra for (a) HPW·nH$_2$O; (b) TSPEN ormosil; and (c) APTS ormosil.

dosimetry. Still, the overall behavior of the band intensity with the dose is nonlinear.

3.2. NMR Spectroscopy. *3.2.1. ^{31}P NMR.* Figure 5 shows the ^{31}P NMR spectra for samples of hydrated HPW (HPW·nH$_2$O) and TSPEN/APTS ormosils. The ^{31}P spectra for both ormosils have a single line centered at −15.3 ppm with fwhm of 0.52 ppm and 0.48 ppm, respectively, for TSPEN and APTS ormosils. The chemical shift is close to that observed in HPW·nH$_2$O (−14.9 ppm, fwhm = 0.07 ppm), which is also consistent with litera-ture data,[39] indicating the integrity of HPW polyanion in the ormosils. The small but consistent chemical shift difference of 0.4 ppm between each ormosil and the HPW·nH$_2$O sample may be attributed to differences in the coordination environments of the polyanions. The broadening of the resonances may be associated to the disordered nature of the ormosils. Nevertheless, the ob-servation of single resonances well separated from the HPW·nH$_2$O line indicates that the polyanions in the ormosils are homogeneously dispersed, with no segregation of pure hydrate-like regions.

Cross-polarization {^{1}H}-^{31}P MAS NMR experiments were carried out at room temperature to probe qualita-tively the effective dipolar coupling between ^{31}P and the ^{1}H nuclei surrounding the polyanion. No {^{1}H}-^{31}P CP MAS signal was observed in the HPW·nH$_2$O sample. Static ^{31}P experiments (direct polarization) at −86 °C

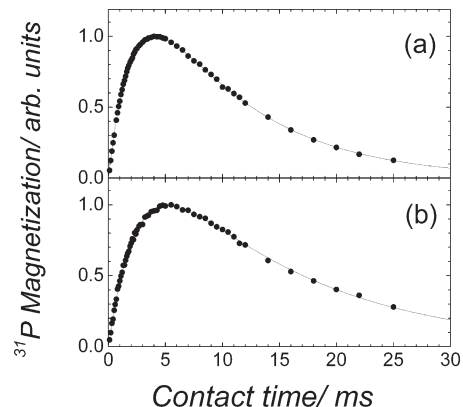(39) Kozhevnikov, I. V.; Sinnema, A.; Jansen, R. J. J.; van Bekkum, H. *Catal. Lett.* **1994**, *27*, 187.

Figure 6. Magnetization curves for CP MAS {^{1}H}-^{31}P NMR experi-ments, using variable contact time. (a) TSPEN ormosil; (b) APTS ormosil. Lines: least-squares fittings of eq 1.

showed a NMR line broadened (fwhm = 900 Hz) with respect to room temperature (fwhm = 400 Hz), revealing the mobility of the polyanion at higher temperatures. Also, a weak {^{1}H}-^{31}P CP signal can be observed for tem-peratures below 80 °C. Therefore, the absence of the cross-polarization signal in hydrated HPW at room tem-perature seems related to the dynamical averaging of the ^{1}H-^{31}P dipolar coupling. In contrast, a strong {^{1}H}-^{31}P CP MAS signal was observed in both ormosil samples at room temperature. Therefore, there is an appreciable effective ^{1}H-^{31}P dipolar coupling, which reveals a state of restricted mobility of the polyanion and the neighbor-ing protons as compared with the hydrated HPW.

Figure 6 shows the spectral intensity in the {^{1}H}-^{31}P CP MAS experiment as a function of the contact time, for a Hartman−Hahn condition of B_1 = 50 kHz. The evolu-tion of the signal may be analyzed considering the ther-modynamic model for cross-polarization from a system of abundant I spins to the observation species S:[40]

$$M_S(t) = \frac{M_{S0}}{a_+ - a_-}(e^{-t/T_{IS}a_-} - e^{-t/T_{IS}a_+}) \qquad (1)$$

with the definitions of

$$a_\pm = a_0\left(1 \pm \sqrt{1 - 2\frac{T_{IS}}{a_0 T_{1\rho}^{(I)}}}\right) \quad \text{and}$$

$$a_0 = \frac{1}{2}\left(1 + \frac{T_{IS}}{T_{1\rho}^{(I)}}\right)$$

where S and I correspond in these experiments to ^{31}P and ^{1}H nucleus, respectively. In eq 1, $M_S(t)$ is the S-spin magnetization after a contact time t, and M_{S0} has a magnitude given by the product between the S-spin magne-tization at thermal equilibrium and the ratio γ_I/γ_S, γ_I and γ_S being the gyromagnetic ratios of the species I and S, respectively. T_{IS} is the characteristic time for cross relaxa-tion, and $T_{1\rho}^{(I)}$ is the spin−lattice relaxation time in the rotating frame for I spins. Table 1 shows the values of the characteristic times T_{HP} and $T_{1\rho}^{(H)}$, obtained from

(40) Mehring, M. *Principles of High Resolution NMR in Solids*; Springer-Verlag: Berlin, 1983.

Table 1. Characteristic Times T_{HP} and $T_{1\rho}^{(H)}$ for {^{1}H}-^{31}P Cross-Polarization in Both Ormosils

sample	$T_{1\rho}^{(H)}$ (ms)	T_{HP} (ms)
TSPEN ormosil	11.0 ± 0.1	2.0 ± 0.1
APTS ormosil	15.8 ± 0.2	2.5 ± 0.1
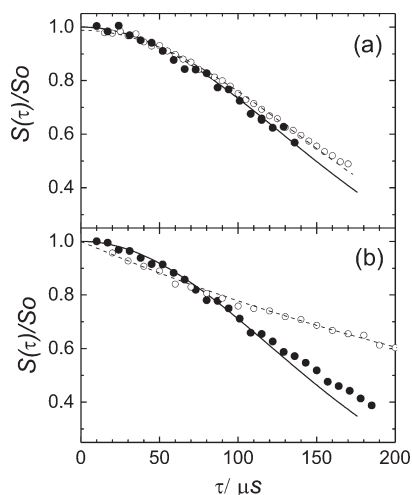
Figure 7. Normalized {^{1}H}-^{31}P SEDOR signal S/S_0 at -80 °C ($\bullet$) and room temperature ($\circ$) as a function of evolution time for (a) TSPEN ormosil and (b) APTS ormosil. Full lines: least-squares fittings using eq 2 with $R = 0.9898$, SD $= 0.015$, and $R = 0.9912$, SD $= 0.011$, respectively, for TSPEN and APTS. Dashed lines: guides to the eye for room temperature data.

least-squares fittings of expression 1 to the data shown in Figure 6. Similar values of T_{HP} and $T_{1\rho}^{(H)}$ are determined in both ormosils, indicating similar effective dipolar coupling and relaxation dynamics, respectively.

3.2.2. ^{31}P-{^{1}H} SEDOR. The SEDOR experiment might give additional insight on the H environment around P in both ormosils. Figure 7 shows the behavior of the ^{31}P-{^{1}H} SEDOR ratio $S(\tau)/S_0$ as a function of the dephasing time τ for both ormosils, measured at low temperature (-80 °C) to suppress possible dynamic effects affecting the ^{1}H-^{31}P dipolar coupling. For TSPEN ormosil, the results were equivalent at room and low temperatures, indicating negligible modulation of the dipolar coupling by molecular motions. On the other hand, for APTS ormosil, there were differences in the SEDOR evolution at room and low temperatures, revealing the existence of dynamic processes reducing the ^{1}H-^{31}P dipolar coupling. Hahn spin−echo experiments (not shown) carried out in this sample confirmed this phenomenon, showing a decay of the echo intensity of exponential type at room temperature and of Gaussian type at low temperature. These two kinds of echo decay are characteristics, respectively, of fast modulation of the dipolar coupling by molecular motions and of the rigid-lattice regime.[41] For short evolution times, the relative SEDOR intensity for a multispin coupling follows a Gaussian relation given by[35,42]

$$\frac{S(\tau)}{S_0} = e^{-2M_{2(HP)}\tau^2} \quad (2)$$

(41) Abragam, A. *The Principles of Nuclear Magnetism*; Clarendon Press: Oxford, 1983.
(42) Boyce, J. B.; Ready, S. E. *Phys. Rev. B* **1988**, *38*, 11008.

Table 2. Second Moment Values $M_{2(HP)}$ of the Heteronuclear ^{31}P-^{1}H Magnetic Dipolar Coupling in Ormosils and Reference Compounds

sample	$M_{2(HP)} \times 10^6$ rad^2 s^{-2}
TSPEN ormosil	15.4 ± 0.4
APTS ormosil	17.2 ± 0.4
$H_3PW_{12}O_{40}$	3.5^a
$H_3PW_{12}O_{40} \cdot 6H_2O$	16.0^b

^{a} Experimental value from ref 33. ^{b} Calculated from crystallographic data in ref 45.

where $M_{2(HP)}$ is the second moment of the dipolar interaction between a central ^{31}P nucleus and the neighboring ^{1}H nuclei, which according to the van Vleck expression for a powder is [41,43]

$$M_{2(IS)} = \frac{4}{15}\left(\frac{\mu_0}{4\pi}\right)^2 I(I+1)\gamma_I^2\gamma_S^2\hbar^2 N^{-1}\sum_{i,j}\frac{1}{r_{ij}^6} \quad (3)$$

The observed low-temperature SEDOR decays in Figure 7 are Gaussian for both ormosils up to intermediate decay ratios, indicating a rigid lattice regime for the ^{1}H-^{31}P dipolar coupling. Least-squares fittings of expression 2 yielded the $M_{2(HP)}$ values shown in Table 2: $(15.4 \pm 0.4) \times 10^6$ rad^2 s^{-2} for the TSPEN ormosil and $(17.2 \pm 0.4) \times 10^6$ rad^2 s^{-2} for the APTS ormosil. Both values are very similar, indicating a comparable number of ^{1}H neighbors and ^{31}P−^{1}H distances. These dipolar couplings can be compared with values corresponding to two different scenarios: the anhydrous HPW and the hydrated form HPW·6H$_2$O. In the first case, a value of $M_{2(HP)} = 3.5 \times 10^6$ rad^2 s^{-2} resulted from the ^{31}P-{^{1}H} SEDOR data presented in ref 35 , which was attributed to the coupling of ^{31}P with three protons bond preferentially to O$_{edge}$ sites of the polyanion. The O$_{edge}$ sites were chosen as the most probable sites for protonation according to the study by Ueda et al.[35] For the second compound, a value of $M_{2(HP)} = 16.0 \times 10^6$ rad^2 s^{-2} was calculated using the crystallographic data of HPW·6H$_2$O in ref 44 and the van Vleck expression 3 . In this compound, the polyanion is surrounded by six dioxonium ions $(H_2O-O-OH_2)^+$ determining an environment around ^{31}P composed by 56 protons with P−H distances within 6.1 Å and 6.5 Å.[44,45] The $M_{2(HP)}$ values measured in both ormosils indicate that the polyanions have a high number of ^{1}H neighbors, the same order of magnitude as observed in the HPW·6H$_2$O compound. In the ormosils, nitrile groups (—C≡N), as unprotonated and protonated primary and secondary amine groups (R-NH$_2$, R-NH$_3^+$, R$_2$-NH, and R$_2$-NH$_2^+$, respectively), hydrate species, and propyl groups may contribute with protons around the polyanion. Considering a common value for ^{31}P−^{1}H distances of 6.32 Å for the closer protons, which is the average of P−H distances in HPW·6H$_2$O, a van Vleck calculation yields a rough estimation of 53 and 59 protons surrounding the polyanion,

(43) van Vleck, J. H. *Phys. Rev.* **1948**, *74*, 1168.
(44) Kremenovic, A.; Spasojevic-de Biré, A.; Dimitrijevic, R.; Sciau, P.; Mioé, U. B.; Colomban, Ph. *Solid State Ionics* **2000**, *132*, 39.
(45) Kremenovic, A.; Spasojevic-de Biré, A.; Bourée, F.; Colomban, Ph.; Dimitrijevic, D. M.; Mioc, U. B. *Solid State Ionics* **2002**, *150*, 431.

respectively, for TSPEN and APTS ormosils. Therefore, it can be concluded that the coordination environment of the polyanions in the ormosils is composed of more than 50 H atoms.

3.2.3. ^{29}Si NMR. Figure 8a,c shows the ^{29}Si MAS NMR spectra for the ormosils. The resonance lines were attributed to silicon species according to the values of chemical shift found in the literature. Tetrahedral silicate species Q^n, establishing n Si−O−Si bonds per tetrahedron, were identified in the spectra with $n = 2 (\sim−91.5$ ppm), $n = 3 (\sim−101.5$ ppm), and $n = 4 (\sim−110.5$ ppm).[46] Two siloxane species with Si−C bonds were also identified, according to their chemical shift, and the results of HETCOR experiments (Section 3.2.4): T^3 species $(SiO)_3Si*(R)$ ($−67$ ppm) and T^2 species $(SiO)_2Si*OHR$ ($\sim−58$ ppm), with R corresponding to the aminopropyl chain of each compound.[47−50] The populations of each silicon species were obtained from least-squares fittings of Gaussian functions to the ^{29}Si NMR spectra. The resulting fractions are summarized in Table 3. According to these results, the difference in the populations of both ormosils corresponds to the increase in the fraction of T^2 species in the APTS ormosil, at the expense of fewer Q^2 and Q^3 sites. The overall condensation degree of the ormosil matrix may be quantified calculating the average number of Si−O−Si bonds per tetrahedron, using the silicon populations from Table 3, resulting in 3.2 for both samples.

Figure 8b,d shows $\{^1H\}$-^{29}Si CP MAS NMR spectra with appreciable intensities for all silicon sites, obtained with a Hartman−Hahn condition of $B_1 = 71$ kHz. Even Q^4 sites are polarized, which indicate that many of these species should be establishing Si−O−Si bridges with other units bringing ^1H nuclei into proximity, as Q^n of lesser connectivity, T^2 or T^3. This observation reveals that in both ormosils there are no extended silica-like Q^4 domains. Figure 9 shows the intensity of the $\{^1H\}$-^{29}Si

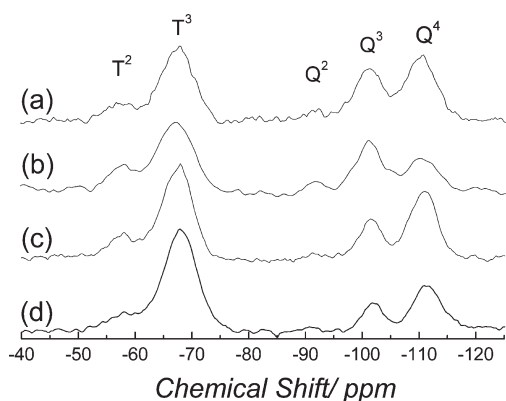cross-polarization signal as a function of the contact time for the most intense and resolved lines (T^3, Q^3, and Q^4). Least-squares fittings of expression 1 were carried out, resulting in the values of T_{HSi} and $T_{1\rho}^{(H)}$ shown in Table 4. For each ormosil, the values of contact times T_{HSi} follow a trend according to the expected intensity in dipolar coupling of each silicon species: the longest values are for Q^4 silicon, while the shortest ones correspond to T^3. In the APTS ormosil the values of contact times T_{HSi} are about half of those in TSPEN ormosil, for each species. This fact indicates that the effective ^1H-^{29}Si dipolar coupling is about two times stronger for silicon sites in the APTS than in the TSPEN ormosil. The values for spin−lattice relaxation time $T_{1\rho}^{(H)}$ in the TSPEN ormosils are different for each site, revealing a spatial separation between these proton systems. This may indicate some degree of heterogeneity at a nanometric scale in the inorganic network. In contrast, for the APTS sample the values are quite similar, a situation that could be compatible with a homogeneous coupling between all protons polarizing the silicon species.

3.2.4. $\{^1H\}$-^{29}Si HETCOR. These experiments may shed light into the question whether the protons polarizing different silicon species constitute a homogeneous reservoir or if they are physically separated. Figures 10
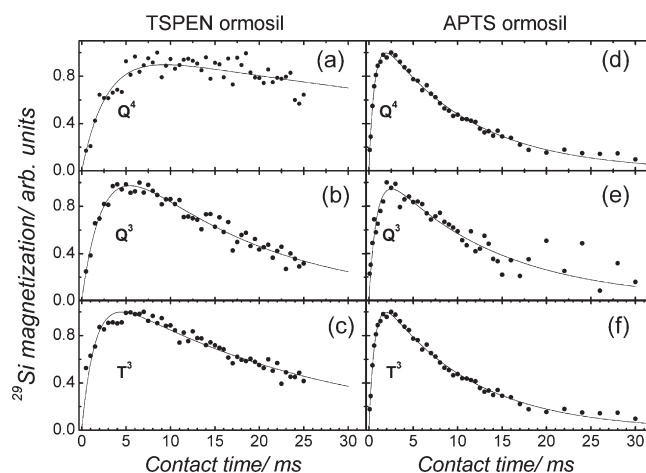
Figure 9. Evolution of the ^{29}Si spin magnetization as a function of contact time for CP $\{^1H\}$-^{29}Si NMR experiments. (a) Q^4, (b) Q^3, and (c) T^3 sites in TSPEN ormosil and (d) Q^4, (b) Q^3, and (c) T^3 sites in APTS ormosil. Full lines: least-squares fittings of eq 1.

Table 4. Characteristic Times T_{HSi} and $T_{1\rho}^{(H)}$ for $\{^1H\}$-^{29}Si Cross-Polarization in Both Ormosils

	TSPEN ormosil		APTS ormosil	
site	T_{HSi} (ms)	$T_{1\rho}^{(H)}$ (ms)	T_{HSi} (ms)	$T_{1\rho}^{(H)}$ (ms)
T_3	$1.5 \pm 0,1$	24 ± 1	0.66 ± 0.03	10.1 ± 0.2
Q_3	2.4 ± 0.2	16 ± 1	0.9 ± 0.1	13 ± 1
Q_4	3.6 ± 0.5	43 ± 9	1.7 ± 0.1	15 ± 9

Figure 8. ^{29}Si MAS NMR spectra in direct polarization for (a) TSPEN and (c) APTS ormosils. Cross-polarization $\{^1H\}$-^{29}Si MAS NMR spectra for (b) TSPEN and (d) APTS ormosils.

Table 3. Isotropic Chemical Shift δ and Populations I of Silicon Species in Ormosils, Determined from ^{29}Si NMR

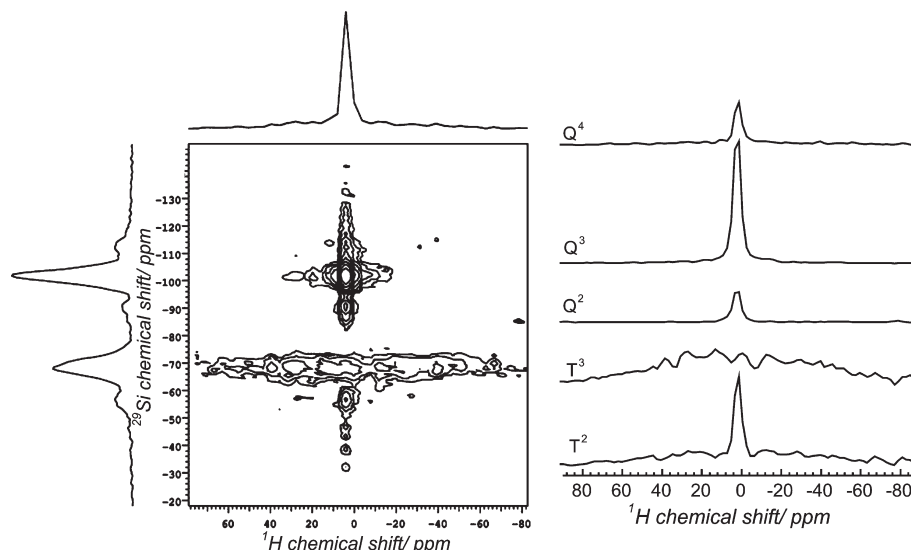|	T^2		T^3		Q^2		Q^3		Q^4	
sample	δ (ppm)	I (%)	δ (ppm)	I (%)	δ (ppm)	I (%)	δ (ppm)	I (%)	δ (ppm)	I (%)
TSPEN ormosil	−57.4	8	−67.4	37	−91.7	3	−101.1	22	−110.4	30
APTS ormosil	−57.9	14	−68.0	40	−91.5	1	−101.5	14	−110.9	31

Figure 10. 2D {^{1}H}-^{29}Si HETCOR spectrum of the TSPEN ormosil. Vertical axis: ^{29}Si chemical shift dimension. Horizontal axis: ^{1}H chemical shift. Slices on the ^{1}H frequency correspond to the main silicon resonances. Integrated projections are shown on the respective axis of the 2D spectrum.
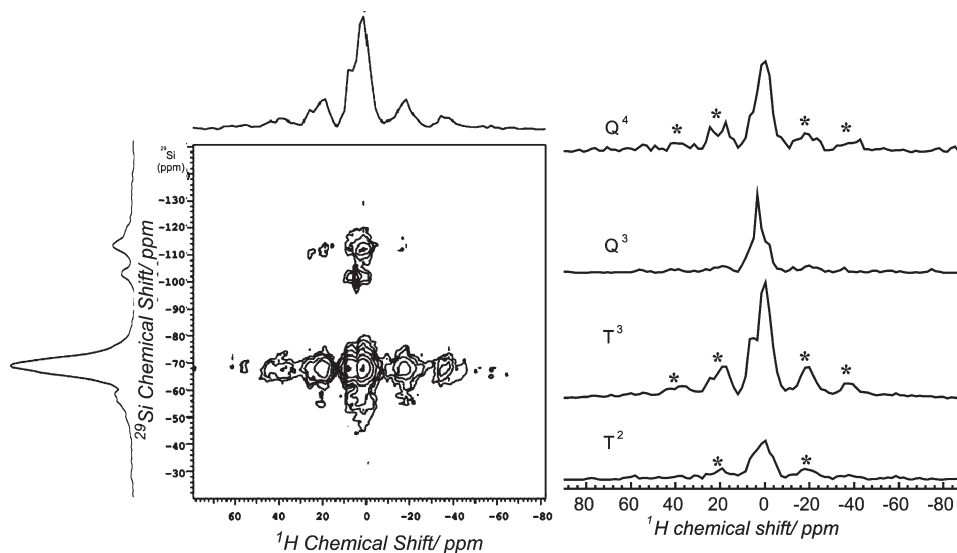

Figure 11. 2D {^{1}H}-^{29}Si HETCOR spectrum of the APTS ormosil. Vertical axis: ^{29}Si chemical shift dimension. Horizontal axis: ^{1}H chemical shift. Slices on the ^{1}H frequency correspond to the main silicon resonances. Integrated projections are shown on the respective axis of the 2D spectrum.

and 11 show the 2D HETCOR spectra for the ormosils and the slices across the ^{1}H frequencies taken at the position of the strongest ^{29}Si resonances. These ^{1}H subspectra show differences in line-width and the intensity of MAS side-bands, both characteristics related to the strength of the proton−proton dipolar coupling. For the TSPEN ormosil (Figure 10) the HETCOR slices along the ^{1}H frequency for Q^4, Q^3, and Q^2 species show narrow ^{1}H lines (fwhm = 2 kHz) without any appreciable spinning side-bands, which means very low ^{1}H homonuclear

coupling, as would be the case of isolated silanol, that is, Si−OH groups far from other protons. In contrast, the ^{1}H slice for Q^4 species in the APTS ormosil (Figure 11) shows two ^{1}H resonances (0 ppm and 5 ppm) with well-resolved spinning side-bands, which indicates a moderate ^{1}H homonuclear coupling for both proton species. The total fwhm of this center-band is 3 kHz. The higher frequency resonance may be attributed to OH protons and the lower one to C−H protons. For Q^3 species, the ^{1}H-spectrum of polarizing protons shows a line at 5 ppm with a partially resolved shoulder (0 ppm) and no spinning sidebands (fwhm = 1.5kHz). This may also indicate two types of polarizing protons, OH and protons from the aminopropylic chains H_{ap} (H−C or H−N protons), both having weak homonuclear coupling. With respect to the siloxane species T^2 and T^3, major differences in the ^{1}H-spectra of both ormosils can be noticed. In the TSPEN ormosil, a very broad ^{1}H subspectrum (fwhm = 40 kHz) is

(46) Engelhardt, G.; Michel, D. *High-Resolution Solid-State NMR of Silicates and Zeolites*; John Wiley & Sons: Chichester, 1987.
(47) De Haan, J. W.; van den Bogaert, H. M.; Ponjeé, J. J.; van De Ven, L. J. M. *J. Colloid Interface Sci.* **1986**, *110*, 591.
(48) Williams, E. A. *Annu. Rep. NMR Spectrosc.* **1984**, *15*, 235.
(49) Harris, R. K.; Kennedy, J. D.; McFarlane, W. *NMR and the Periodic Table*; Academic Press: London, 1978.
(50) Peeters, M. P. J.; Walkelkanp, W. J. J.; Kentgens, A. P. M. *J. Non-Cryst. Solids* **1995**, *189*, 77.
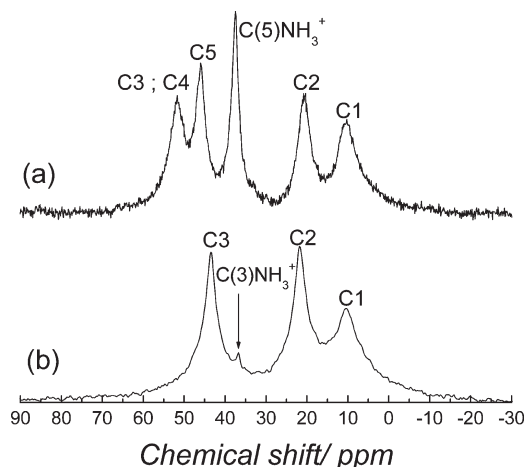
Article

Chem. Mater., Vol. 23, No. 4, 2011 961

Figure 12. $\{^1H\}$-^{13}C cross-polarization NMR spectra for (a) TSPEN ormosil and (b) APTS ormosil and the attributions for the observed resonances according to notation in Scheme 1.

Table 5. Isotropic Chemical Shifts and Attributions for Observed Resonances in Cross-Polarization $\{^1H\}$-^{13}C NMR Spectra for TSPEN and APTS Ormosils[a]

TSPEN ormosil		APTS ormosil	
attributions	δ (ppm)	attributions	δ (ppm)
C_1	10.4	C_1	10.5
C_2	20.7	C_2	21.8
$C_5\ NH_3^+$	37.6	$C_3\ NH_3^+$	36.8
$C_5\ NH_2$	46.1	$C_3\ NH_2$	43.5
C_3, C_4	51.7		

[a] Carbon identifications correspond to the labeling in Scheme 1.

Scheme 1. Structural formulae of TSPEN and APTS Molecules

observed for T^3 species. In this case, the MAS at 7 kHz is unable to reduce the line-width, revealing the existence of a strong homonuclear dipolar coupling between these protons. In contrast, the ^1H subspectrum for the T^3 slice in the APTS ormosil shows a center-band with two narrower signals (0 ppm and 5 ppm, total fwhm = 3.5kHz) with a resolved set of side-bands, indicating moderate ^1H homonuclear coupling. These proton resonances correspond to OH and H_{ap}. For T^2 species in TSPEN, an intense narrow center-band (fwhm = 1.7kHz) without side-bands is observed in the ^1H subspectrum, indicating weakly coupled protons as in Si–OH groups. The wide baseline observed in this ^1H slice is attributed to the partial spectral overlap with the strong signal from the protons associated with T^3 species. This led us to attribute the T^2 silicon specifically to $(SiO)_2Si^*(OH)R$, instead of $(SiO)_2Si^*(OMe)R$. The latter possibility is excluded because methyl protons in a restricted mobility state, a condition necessary to cross-polarize silicon, should have a considerably broadened ^1H resonance. Therefore, T^2 species in this ormosil seem to be originated from hydrolysis. In the APTS ormosil, the ^1H slice corresponding to T^2 silicon shows a broader line, which may encompass OH and H_{ap} protons, having resolved side-bands indicating moderate homonuclear coupling. The possible attributions of these T^2 silicons are either $(SiO)_2Si^*(OH)R$ or $(SiO)_2Si^*(Et)R$. Considering the ^{13}C NMR spectrum of this ormosil (Section 3.2.5), the latter possibility seems to be less probable because no clear signal of CH_3 carbons can be resolved.
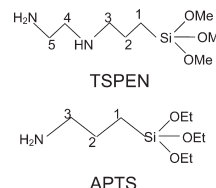
3.2.5. ^{13}C NMR. Figure 12 shows the $\{^1H\}$-^{13}C cross-polarization NMR spectra of both ormosils. Table 5 shows the chemical shift of the NMR lines and their attributions, following identifications in Scheme 1, according to literature data.[51,52] The ^{13}C signals agree with the expected carbons in the aminopropylic chain in each ormosil, indicating the integrity of these molecular

fragments. Signals from the carbon in $Si–O–C^*H_2$-R groups are not observed in any ormosil, demonstrating the complete reaction of these species. An additional intense resonance at 37 ppm observed in the spectrum of the TSPEN ormosil was attributed to CNH_3^+. A weak line can be observed at the very same position in the spectrum of the APTS ormosil, demonstrating the extremely small population of these species in this sample.

3.2.6. ^{31}P NMR on Irradiated Samples. Figure 13 shows the ^{31}P NMR spectra of both ormosils before (parts a and d) and after UV irradiation. Spectra taken immediately after the irradiation, Figure 13b,e, show consistently the presence of a new weak ^{31}P resonance at −10.7 ppm, which can be attributed to those polyanions where the photoreduction process took place. Indeed, Kazansky and McGarvey reported the chemical shift for the one-electron reduced specie $[PW_{12}O_{40}]^{4-}$ at −10.4 ppm.[30] Spectra taken 20 h after the irradiation, Figure 13c,f, keeping the samples packed in NMR sample holders open to the atmosphere, do not show this ^{31}P line. The observation of this reversibility justifies the attribution of the new resonance to the reduced state and not to any potential decomposition of the polyanion due to sample heating. Yet, the NMR lines in Figure 13c,f are slightly broadened compared to the state before irradiation, also showing a low intensity shoulder at around −13 ppm. These signals could indicate the in situ formation of a slight fraction of Wells-Dawson polyoxometalate $[P_2W_{21}O_{71}]^{6-}$,[53,54] but the intensity and resolution are too low for a precise identification.

4. Discussion

The photochromism of POM is based on the formation of a charge transfer complex between proton donor species, such as alkylammonium, protonated amines, and

(51) Shimizu, I.; Okabayashi, H.; Hattori, N.; Taga, K.; Yoshino, A.; O'Connor, C. J. *Colloid Polym. Sci.* **1997**, *275*, 293.
(52) Macomber, R. S. *A Complete Introduction to Modern NMR Spectroscopy*; John Wiley & Sons: New York, 1988.

(53) Smith, B. J.; Patrick, V. A. *Aust. J. Chem.* **2004**, *57*, 261.
(54) Kozhevnikov, I. V.; Kloetstra, K. R.; Sinnema, A.; Zandbergen, H. W.; van Bekkum, H. *J. Mol. Catal. A: Chem.* **1996**, *114*, 287.
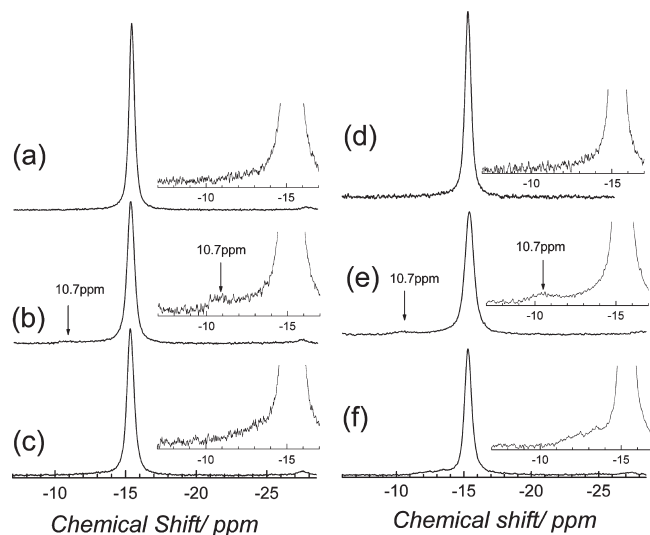
Figure 13. ^{31}P NMR spectra from irradiated ormosils: APTS (a) non-irradiated, (b) irradiated for 30 min, and (c) 20 days after irradiation and TSPEN (d) nonirradiated, (e) irradiated for 30 min, and (f) 20 days after irradiation.

ammonium groups, and the excited phosphotungstate leading to reduced phosphotungstate species.[6,37] Therefore, the presence of such reduced phosphotungstate species in the irradiated ormosils, as revealed in the electronic spectra, is expected and was also observed in other photochromic materials based on phosphotungstate.[55] However, these ormosils doped with HPW showed a different line shape for the spectra after irradiation when compared to the hybrids composed of polyacrylamide-doped phosphotungstate reported by Feng in ref 55. In those irradiated hybrids, a typical electronic spectrum for the reduced phosphotungstate shows the more intense peak between 650 and 750 nm, while our spectra showed more intense bands at lower (APTS) and higher (TSPEN) wavelengths. Such differences in line shape can be attributed to the formation of mono- and bireduced species in our experiments when compared to singly reduced species in the polyacrylamide films. The increase in the higher wavelength peak in the irradiated TSPEN ormosil indicates a better stabilization of the double-reduced phosphotungstate in this hybrid compared to the APTS one. Such stabilization of highly reduced species can be explained by the presence of two amine groups in the TSPEN backbone against one in the APTS. These amine groups are transformed by protonation into ammonium groups able to neutralize the negative charges in the heteropolyblues. Thus, the siloxane with higher number of amine groups is expected to better stabilize the highly reduced heteropolyblues.

The set of NMR experiments indicates that the HPW polyanion is located in an environment with many close protons. The measured ^{31}P chemical shift in both ormosil samples (−15.3 ppm) is closer to hydrated compounds (−14.9 ppm) than to the anhydrous forms (crystalline: −10.8 ppm, amorphous −12 ppm).[29] This is consistent

(55) Feng, W.; Ding, Y.; Liu, Y.; Lu, R. *Mater. Chem. Phys.* **2006**, *98*, 347.

with the SEDOR results at low temperature, revealing a strong dipolar coupling between the central ^{31}P nuclei in the polyanion and a high number of protons (above 53) within a distance of approximately 6.3 Å. The H-environment around the polyanion may be composed of protons from amino or ammonium groups, H_2O, and the propylic chains. Despite the similarity in the structural environments of the HPW in both ormosils, dynamic effects are operative at room temperature in the APTS ormosil, decreasing the effective dipolar coupling between ^{31}P and some [1]H. The higher mobility in the APTS ormosil when compared to the TSPEN ormosil is probably related to the "chelating" effect that TSPEN can provide due to the presence of two nitro groups that interact through electrostatic forces with the phosphotungstate. This interaction by two points of the protonated amino groups in the TSPEN with the phosphotungstate results in a loss of the degree of freedom of the system (lower entropy) with an increase in the strength of the ionic interaction between the siloxane and polyoxometalate (higher enthalpy). Furthermore, this difference in the binding mode between the APTS and TSPEN with the phosphotungstate is responsible for the differences in the electronic spectra of irradiated samples discussed above. The higher photochromic response of the TSPEN ormosil, as indicated by the higher spectral intensities for the band around 740 cm^{-1} as shown in Figure 3, can also be explained by the chelate binding mode of the TSPEN, better stabilizing the photoreduced species or providing more protons to allow the formation of the charge transfer complex between the excited phosphotungstate and the ammonium groups.[38]

The appearance of a high-frequency new peak in the ^{31}P NMR spectrum upon irradiation (−10.7 ppm) is consistent with the photoreduction process. In the one-electron reduced polyanions there is a paramagnetic shift of the ^{31}P resonance due to the delocalized electron.[30] The low intensity of this resonance may indicate that a small fraction of the polyanions participated in the photoreduction process, probably due to low efficiency of the irradiation of the powdered sample and to the low penetration of the radiation in the grains.

^{29}Si MAS NMR shows similar distributions of T^n and Q^n species in both ormosils, with comparable average connectivity of the silica matrix according to the average number of Si−O−Si bridges per tetrahedron. On the other hand, {[1]H}-[29]Si CP and HETCOR experiments reveal significant structural differences between both ormosils at medium-range scale. Basically, the Q^n silicon species in the TSPEN ormosil seem to be structurally separated from T^3 species, while in the APTS ormosil there is a higher degree of mixing between Q^n and T^n. Scheme 2 summarizes the correlation map obtained from HETCOR and cross-polarization experiments. Two kinds of polarizing protons were identified: OH, from silanol or water molecules, and protons from the aminopropylic chains H_{ap} (H−C or H−N species). The full arrows in Scheme 2 connect species with sizable [29]Si−[1]H dipolar coupling, while the dotted arrows connect species showing weaker dipolar correlation. Let us discuss first the correlations in

TSPEN ormosil

Q^2

Q^3 — HO → T^2

Q^4 — H$_{ap}$ → T^3

APTS ormosil

Q^3 — HO → T^2

Q^4 — H$_{ap}$ → T^3
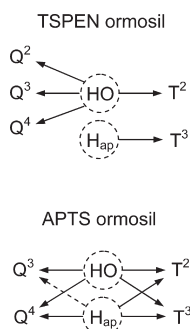
^{a} Full arrows connect species with sizable ^{29}Si−^{1}H dipolar coupling, while dotted arrows connect species showing weaker dipolar correlation.

TSPEN ormosil. According to the HETCOR spectrum in Figure 10, Q^n and T^2 species interact only with isolated OH protons. This condition indicates local configurations maximizing the H−H distances between OH groups in Q^2 and between the H$_{ap}$ and OH in T^2. For the T^3 silicon, which should be interacting with H$_{ap}$, the HETCOR section reveals the strong homonuclear coupling of these protons. Therefore, the OH protons are decoupled from those in the aminopropylic chains, indicating spatial separation of these groups. Consequently, there is a separation of T^3 with respect to the other silicon species. This medium-range structural heterogeneity can be noticed also in the relaxation times $T_{1\rho}^{(H)}$, which are different for Q^n and T^3, indicating separate ^{1}H reservoirs polarizing these silicon species. Another dynamic difference may be noticed within the set of OH bond to Q^3 units. The subset of those protons polarizing Q^4 silicon have a $T_{1\rho}^{(H)}$ value of 43 ms, which is considerably longer than the value for those OH polarizing the majority of Q^3 species (16 ms). This may indicate a separation of Q^3 units linked to Q^4 with respect to the others. On the other hand, the APTS ormosil reveals a more uniform mixture of Q^n and T^n species. The HETCOR spectrum (Figure 11) indicates that, to some extent, OH and H$_{ap}$ polarize every kind of silicon species. The similarity of the Q^4 and T^3 subspectra reveals the proximity between both silicon species. The Q^3 species seems to be polarized mostly by protons in isolated OH groups, indicating less mixture with T species. The most striking difference between the HETCOR spectra in Figures 10 and 11 is the low homonuclear coupling for protons polarizing T^3 silicon in the APTS ormosil. Two factors may be invoked to explain this reduction in the homonuclear coupling of ^{1}H in the aminopropylic chain. The first one is of structural nature: the presence of fewer neighboring protons (H−C, H−N, or H−O) reducing the intermolecular coupling of the protons in the chains. The second one is of dynamic nature: a fast exchange of protons in the NH$_2$ group. This hypothesis may also explain the weaker intensity of the NH$_3^+$ resonance in the cross-polarized {^{1}H}-^{13}C spectrum of the APTS ormosil compared with the TSPEN ormosil.

5. Conclusion

The set of NMR techniques revealed a structural picture of the two hybrid materials sharing some common features: the same average connectivity for the inorganic network and a dispersion of HPW ions in the ormosil, occupying sites with a high number of close protons (>50). Also, two main structural differences were detected in these materials. First, the HETCOR and CP MAS experiments revealed a homogeneous distribution of silicon species for the APTS hybrid, contrasting with the separation of T^3 species in the TSPEN hybrid. Further experimental work should be developed in order to understand the nature of this heterogeneity and whether it may influence the photocrohromic properties of the ormosil. Second, differences in the molecular dynamics at room temperature indicate that the interaction of the HPW with the surrounding molecular groups is stronger in the TSPEN hybrid than in the APTS one. This behavior is consistent with the presence of more amino groups in the TSPEN, acting as cationic adsorption sites for the HPW polyanion and restricting its mobility. Further experiments with ^{15}N NMR may be helpful to identify the different N-groups in these materials. As the TSPEN hybrid shows more intense photochromic response, these observations are in agreement with the charge transfer mechanism proposed to explain the effect. The photoreduction of phosphotungstic acid trapped in aminomodified ormosil matrices does result in one-electron and two-electron reduced polyanions as evidenced by reflectance electronic spectroscopy. The one-electron heteropolyblue could be detected also by ^{31}P NMR. The population of the one-electron and two-electron heteropolyblue species as a function of the UV dose is dependent on the number of amine groups in the aminosilane grafted in the ormosil. A higher amount of amine groups produces a higher population of two-electron species at lower doses and a steep increase in the population of the one-electron reduced species at higher doses.